Three-Dimensional Fabrication of Micro-/Nanostructure Using Scanning Probe Lithography

13

Yanquan Geng and Yongda Yan

Contents

Abstract

As one of the tip-based nanofabrication approaches, the atomic force microscope (AFM) tip-based nanomechanical machining method has been successfully utilized to fabricate three-dimensional (3D) nanostructure. First, the principle of AFM tip-based mechanical nanomachining is introduced, which includes contact and tapping modes. Second, fabrication of 3D nanostructure by material removal is presented. This part contains force- and feed-control approaches. Third, ripple-type nanostructure machined with stick-slip process is described. This method is usually implemented on the polymer materials. Finally, a novel machining method combining the material pileup and the machined groove to form a 3D nanostructure is presented. It is expected that this chapter will serve to aid in the advance of the fabrication of 3D nanostructure and expand its applications in various fields.

Y. Geng · Y. Yan (✉)
Center for Precision Engineering, Harbin Institute of Technology,
Harbin, Heilongjiang, China
e-mail: yanyongda@hit.edu.cn

13.1   Introduction

With the rapid development of the nanotechnology, more and more nano-structures have been used in various fields, such as nanofluidic (Peng and Li 2016; Duan et al. 2016), nanosensor (Kim et al. 2009; Barton et al. 2010), and nanooptics (Kumar et al. 2012; Dregely et al. 2013). However, how to fabricate the nanostructure with desired dimensions is still a hot and difficult problem. There are a number of methods to produce three-dimensional (3D) nanostructure, including nanoimprint lithography (Liang and Chou 2008), focused ion-beam nanolithography (FIB) (Menard and Ramsey 2011), and electrochemical machin-ing (Zhan et al. 2016). However, due to the properties of complexity, low throughput, and/or cost of implementation, these approaches are restricted for more extensive applications.

The atomic force microscopy (AFM) tip-based nanofabrication method has been proved as a powerful and feasible approach to create nanostructure with high quality, due to the advantages of nanoscale machining accuracy, wide range of applicable materials, atmospheric environment requirement, and low cost (Yan et al. 2015). The AFM tip-based nanofabrication method includes dip-pen nanolithography (Richard et al. 1999), thermochemical nanolithography (Pires et al. 2010), local anode oxidation (Dagata 1995), and nanomechanical machining methods (Yan et al. 2015). The nanomechanical machining method is the easiest and most flexible approach among the various AFM tip-based nanofabrication techniques. Some scholars have utilized this nanomechanical machining method to fabrication nano-groove (Geng et al. 2014), 2D (Brousseau et al. 2013), and 3D (Yan et al. 2010) nanostructures on different materials, such as metal (Geng et al. 2013a), polymer (Geng et al. 2016a), and semiconductor (Lin and Hsu 2012). The fabrication of 3D nanostructure is the most complicated and difficult. Mao et al. found that the material cannot be removed effectively to form the material pileup when using the silicon AFM tip to conduct nanoscratching (Mao et al. 2009). Thus, the authors utilized the material pileup to form 3D nanostructure by controlling the scratching trajectory. Based on this method, a steric Taiwan map has been fabricated (Mao et al. 2009). However, the machining accuracy and repeatability of this method is needed to be improved. Yan et al. used gray-scale map to fabricate human face on the aluminum alloy surface (Yan et al. 2010). They employed a 3D high-precision stage to take the place of the original stage of the AFM. During the machining process, the AFM tip remained stationary, and the motion of the sample is controlled by the 3D high precision using the gray-scale map. The relative displacement between the sample and the AFM tip can result in the change of the deflection of the tip cantilever, which can thus cause the variation of the applied normal load by the AFM tip on the sample surface to achieve the fabrication of 3D nanostructure. However, in this proposed method, the relationship

between the machining parameters and the machined depth was not given. Thus, the dimensions of the machined 3D nanostructure are unpredictable.

In this chapter, we review several approaches to fabricate 3D nanostructure with desired dimensions by using the AFM tip-based nanomechanical machining technique. These methods will advance the application of the AFM tip-based nanomechanical machining technique in various fields.

13.2   Principle of AFM Tip-Based Mechanical Nanomachining

Since the AFM was invented in 1986 by Binnig et al. (1986), it has been considered as a profiler with nano-precision. The interaction force between the tip and the sample surface is usually set as several hundred nano-newtons to guarantee no damage occurring when measuring the target surface. However, when this force increases to several micro-newtons, the plastic deformation of the sample surface may be occurring during the scanning process, especially for the soft materials. Some scholars utilized this principle to conduct nanomachining on the surface with good quality, due to the motion limitation of the AFM PZT in z direction. The mechanical machining mode of the AFM tip-based nanofabrication technique mainly includes contact and tapping modes, which corresponds to the typical scanning modes of the AFM. For the contact mode, the interaction force between the tip and the sample is controlled by the defection of the cantilever of the AFM tip. This applied normal load can be kept constant by adjusting the deflection of the tip cantilever. The deflection of the cantilever is controlled by the motion of the AFM PZT in z direction through an optical lever system. Thus, to achieve 3D nanostructure, one method can be changing the applied normal load according to the corresponding machined depth by controlling the vertical motion of the AFM PZT in z direction. The applied normal load can be calculated by:

$$F_{\mathrm{N}} = K_{\mathrm{N}} \cdot s \cdot V_{\mathrm{setpoint}} \qquad (1)$$

where K_{N} is the normal spring constant of the tip cantilever, s is the sensitivity of the position sensitive detector (PSD), and V_{setpoint} is represented the vertical voltage value preset by the user. The product of s and V_{setpoint} is the deflection of the tip cantilever in the vertical direction. Thus, the applied normal load can be controlled by the preset value of V_{setpoint} directly.

For the tapping mode, the interaction force is not only related to the properties of the tip and sample including tip radius, spring constant of the tip cantilever, and the mechanical properties of the sample material, but also concerned with the preset machining parameters, such as the driven amplitude, the driving frequency, and the tip-sample distance (Chen et al. 1994; Salapaka et al. 2000; Tamayo and Garcia 1996). The tapping mode of the AFM tip is always assumed as a damping oscillator system. This system is driven by a sinusoidal force, and the substrate is deformable, which can be expressed by (Liu et al. 2012):

$$m\frac{\mathrm{d}^2 z}{\mathrm{d}t^2} = -K_N z - \frac{m\omega_0}{Q}\frac{\mathrm{d}z}{\mathrm{d}t} + F_0 \sin(\omega t) + F(z_c, z) \tag{2}$$

where m is the effective mass of this oscillator system, which can be obtained by K_N/ω_0^2. ω_0 is the angular resonance frequency, and Q is the quality factor of the tip cantilever. The driven force can be expressed as $F_0 \sin(\omega t)$. F_0 can be calculated as $K_N \times A_m$; A_m is the driven amplitude. $F(z_c, z)$ represents the interaction force between the tip and the sample at one position deviated from the center of the vibration in the vertical direction, z, and z_c is the tip-sample separation without the oscillation of the cantilever. In terms of the vertical position z, $F(z_c, z)$ can be divided into two scenarios: when the distance between the tip and the sample is larger than a certain value a_0, the van der Waals model should be employed to obtain $F(z_c, z)$; while, when the tip-sample distance is smaller than this value a_0, the Hertz contact model should be used to calculated $F(z_c, z)$. Thus, $F(z_c, z)$ can be expressed as (Liu et al. 2012):

$$F(z_c, z) = \begin{cases} -\dfrac{AR}{6(z_c + z)^2} & z_c + z > a_0 \\ -\dfrac{AR}{6a_0^2} + \dfrac{4E^*\sqrt{R}}{3}(a_0 - z - z_c)^{3/2} & z_c + z \le a_0 \end{cases} \tag{3}$$

where A is the Hamaker constant. R and E^* are the radius of the tip and the effective Young's modulus of the sample, which can be calculated as:

$$\frac{1}{E^*} = \frac{(1 - \nu^2)}{E} + \frac{(1 - \nu_1^2)}{E_1} \tag{4}$$

where E and ν are the Young's modulus and the Poisson's coefficient of the sample, respectively, and E_1 and ν_1 are the Young's modulus and the Poisson's coefficient of the tip material, respectively.

During the machining process of one structure, the tip and sample are usually prearranged. Thus, the interaction force is always controlled by the machining parameters when implementing nanoscratching using tapping mode, which cannot be obtained directly. Comparison of the contact and tapping modes, it can be observed the interaction force can be controlled more easily by the contact mode, as shown in Eq. 1. For this reason, the contact mode is usually selected to conduct nanofabrication of the 3D nanostructures (Yan et al. 2010). However, due to the intermittent interaction between the tip and the sample, scratching with tapping mode is proved as an efficient approach for reduction of tip wear (He et al. 2018). Therefore, some scholars utilized the tapping mode to carry out a long-term scratching process with a silicon AFM tip (He et al. 2018; Heyde et al. 2001).

The AFM tip-based nanomechanical machining method has been used to fabricate nanostructure on various materials, such as semiconductor, metal, and polymer (Yan et al. 2015). For the semiconductor and metal material, a relatively large normal load is needed to create structures. The tip wear cannot be neglected, especially for

the semiconductor materials due to owning a relatively large hardness. Thus, the diamond- or diamond-like-coated AFM tip is always chosen to reduce the tip wear, while the typical silicon tip is usually selected to scratch on the polymer material. The possible reason can be explained as follows. The polymer material is easy processing due to its small hardness, and the silicon tip is completely competent to carry out a long-term scratching process. Moreover, the radius of the silicon tip is relatively small, which can be used to fabricate nanostructures with more accurate dimensions, and the low price of the silicon tip is another advantage. Therefore, the selection of the tip used for machining is dependent on the sample material.

13.3 Fabrication of 3D Nanostructure by Material Removal

13.3.1 Selection of Feed Direction

In order to fabricate 3D nanostructure, a feed value with a direction perpendicular to the scratching direction is needed to expand the width (Geng et al. 2016b), rather than a single scratch for machining nanoline. Thus, in this case, the normal load is not the only factor for controlling the machined depth. The feed value also has a large influence on the dimensions of the structures. In the machining process of 3D nanostructure, the feed direction is a key factor due to the asymmetrical geometry of the AFM tip, which needs to be studied first. In terms of the tip-sample relative displacement and the geometry of the tip, three typical feed directions, named edge-forward, face-forward, and sideface-forward, are investigated, as shown in Fig. 1. For the edge-forward feed direction, the sample is controlled to move parallel and toward the tip cantilever after a single scratch to complete one feed operation, as shown in Fig. 1a. Oppositely, the sample moves parallel but away from the tip cantilever in the face-forward feed direction, as shown in Fig. 1b. While, for the sideface-forward, the sample is controlled to move perpendicular to the tip cantilever, as shown in Fig. 1c. Due to the feeds are usually selected as very small values, such as tens to hundreds of nanometers, only the corresponding edge or the face of the tip takes part in the scratching process. Taking a diamond tip as an example, the OA edge of the tip, shown in Fig. 1d, participates in the scratching process with the edge-forward feed direction. In the face-forward feed direction, both the edge OB and OC may take part in the scratching process. Thus, we consider plane BOC playing the main role for the material removal. For the sideface-forward feed direction, only the edge OB or OC participates in the scratching process.

In our pervious study (Geng et al. 2016b), scratching tests were carried out on the 2A12 aluminum alloy surface with a diamond AFM tip to study the influence of the feed directions on the machined outcomes. The surface of the sample was per machined by the single-point diamond turning, and the surface roughness can reach 5 nm approximately. Figures 2 and 3 show the SEM and AFM images of the nanochannels machined with the three typical feed directions. The conventional zigzag trajectory was selected. The feed and normal load were set as 120 nm and 67 μN, respectively. The SEM images were taken just after the machining process,
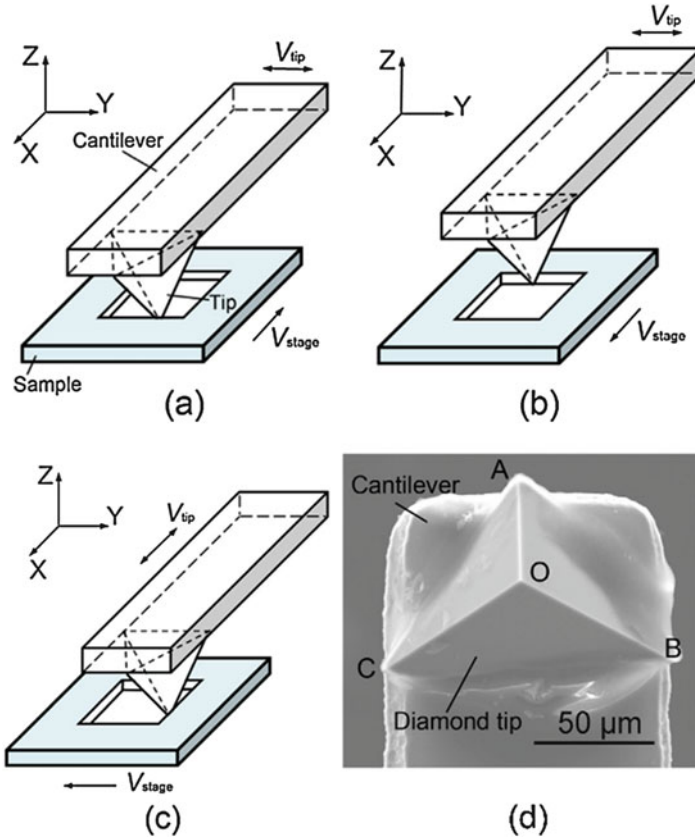
Fig. 1 Three typical feed directions and the SEM image of the diamond tip: (**a**) edge-forward, (**b**) face-forward, (**c**) sideface-forward, and (**d**) SEM image of the tip (Reproduced with permission from Geng et al. 2016b)

and the AFM images were obtained after washing the sample in alcohol solution for about 10 min to remove the chips generated in the machining process. As shown in Fig. 2a and d, continuous chips are formed when scratching with edge-forward feed direction. It can be observed from the magnified image of the chips in Fig. 2d that one side of the chip has a sawtooth shape. This has been explained that both cutting and plowing machining states occur to generate this sawtooth shape (Geng et al. 2016b). However, the formation of the continuous chips indicates that cutting state plays the main role in the machining process. Moreover, it can be found from Fig. 3a that no chip was adhered on the sides of the nanochannel. This means the chips can be washed away easily before scanning by the AFM, which is attributed to the sawtooth shape on one side of the chips. The sawtooth shape can result in the chips being broken easily. From the cross section of the nanochannel shown in Fig. 3a, a nanochannel with relative good quality was obtained when machining by the edge-
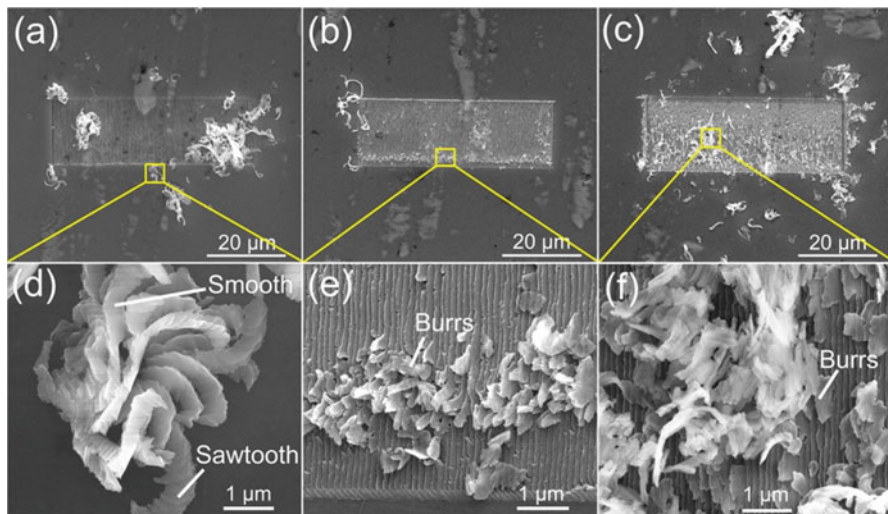
Fig. 2 SEM images of the nanochannels machined with three typical feed directions: (**a**) edge-forward, (**b**) face-forward, and (**c**) sideface-forward (Reproduced with permission from Geng et al. 2016b)

forward feed direction. The machined depth was measured as 208 nm approximately (Geng et al. 2016b). As shown in Fig. 2b and e, prominent burrs can be found in the processed area when implementing scratching process with the face-forward feed direction. From the AFM image shown in Fig. 3b, it can be seen that no obvious depth obtained after machining with the face-forward feed direction. This indicates that the materials cannot be removed effectively, and plowing machining state plays an important role in this case. The possible reason for this is the extremely small attack angle of the main cutting edge (Geng et al. 2016b). Thus, the face-forward feed direction is not suitable for the fabrication of 3D nanostructure. For the sideface-forward feed direction, both the chips and the burrs can be generated during the machining process, as shown in Fig. 2c and f. In this condition, the attack angles of the trace and retrace in the reciprocating motion are different, which are about 26.5° and 63.5°, respectively. For the attack angle of 26.5°, the plowing mechanism may occur, which leads to burr formation, while, in the opposite motion, the attack angle can reach 63.5°, which results in the generation of the chips. However, the clearance angle is estimated only 26.5° in this case. This relatively small clearance angle may not be enough to form the continuous chips. The coexisting of the chips and burrs is attributed to the variation of the attack angles in the reciprocating motion. In addition, it can be observed from Fig. 3c that there is a large variation of the machined depth along the width and length cross section, which is caused by the unitability of the machining process in the reciprocating motions. Thus, considering the consistency of the machined depth and the surface quality, the sideface-forward feed direction is also not suitable for the fabrication of the 3D nanostructure.
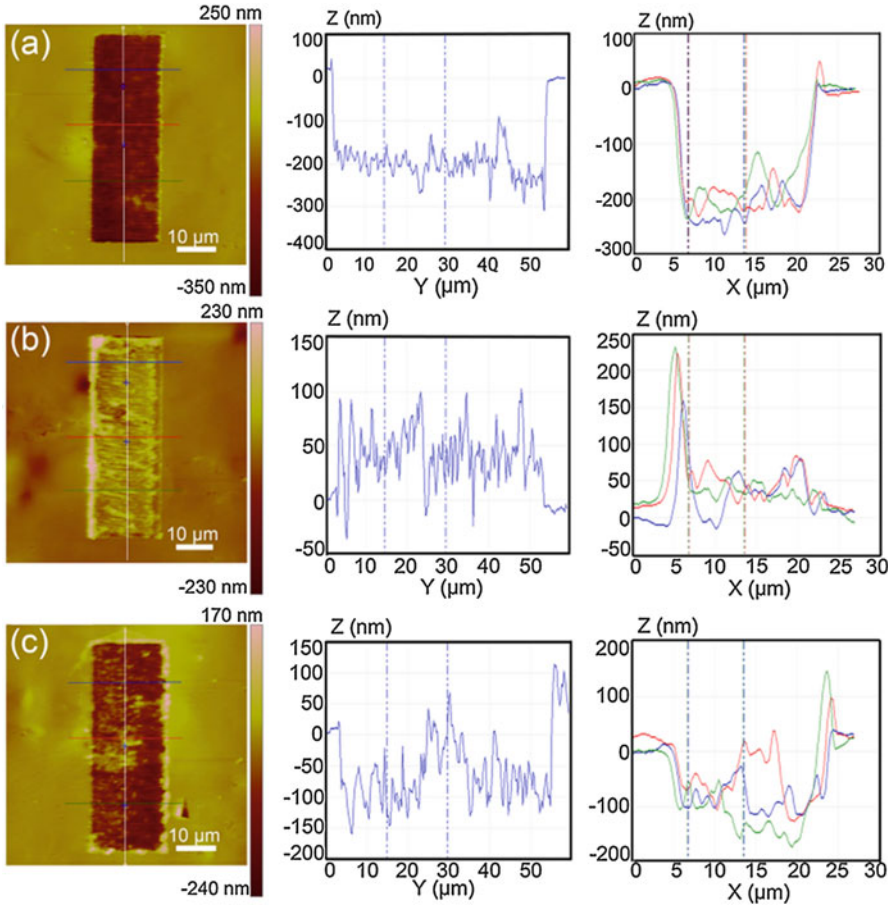
Fig. 3 AFM images and the corresponding cross sections of the nanochannels machined with three typical feed directions: (**a**) edge-forward, (**b**) face-forward, and (**c**) sideface-forward (Reproduced with permission from Geng et al. 2016b)

13.3.2 Fabrication 3D Nanostructure by Controlling the Applied Normal Load

As described in Sect. 3.1, the edge-forward feed direction is the best among the three typical feed directions. Thus, in the machining process of 3D nanostructure, edge-forward feed direction is selected. Moreover, as discussed in Sect. 3.1, the machined depth of the nanostructure is related to the applied normal load and the feed values, which is also studied in our previous study (Geng et al. 2013a). Thus, both the applied normal load and the feed values can be used to control the machined depth to achieve 3D nanostructures. Most scholars utilized the intuitive force-control approach to fabricate nanostructures with fluctuant machined depth, and the feed is kept as a constant value, as shown in Fig. 4a. In order to better understand the
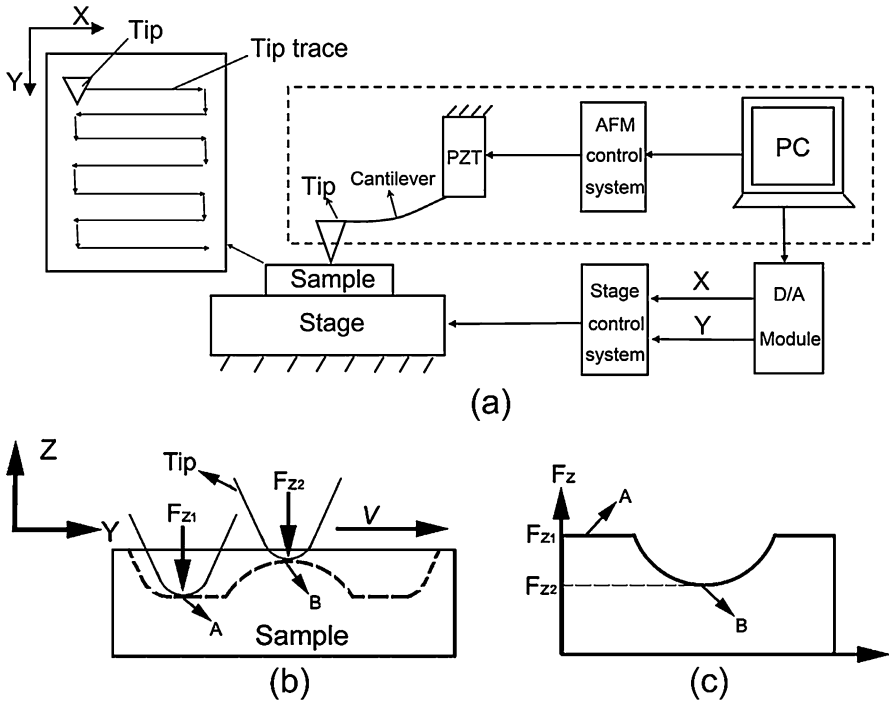
Fig. 4 (**a**) Schematic of the modified AFM tip-based nanomachining system. (**b**) The dotted line shows a 3D nanostructure required to be machined. (**c**) Corresponding force single in machining the 3D nanostructure shown in (**b**) (Reproduced with permission from Yan et al. (2010) and Geng et al. (2013b))

nanomachining process and guarantee the machining quality, a rectangular tip trajectory is usually selected. Unlike the traditional processing, the relationship between the applied normal load and the machined depth should be investigated first for the AFM tip-based nanomachining. It can easily be imagined that the machined depth increases with the normal load going up. Figure 4b shows the cross section of the desired nanostructure, and Fig. 4c illustrates the corresponding normal loads needed to be applied on the surface. It can be observed that the deeper point of the machined depth needs a relatively large normal load. Due to the large pileup formed in the machining process (Geng et al. 2016a), the polymer material is not suitable for this material removal approach to fabricate 3D nanostructure. Thus, the metal is usually selected as the sample material in this method. In the nanomachining process of the metal material, the plastic deformation is the dominant mechanism of energy dissipation (Bhushan 2002), and the influence of the elastic recovery can be neglected. For this reason, the nanomachining process can be treated as a hard particle sliding over a soft sample surface (Geng et al. 2013b). The applied normal load (F_N) can be calculated by the product of the yield pressure of the sample material (σ_p) and the horizontally projected area of the tip-sample interface (A_T), as

expressed in Eq. 5 (Bowden and Tabor 1950). σ_p is the property of the material, which can be obtained by the nanoindentation process. A_T has a relationship with the machined depth (h). Thus, the relationship between F_N and h can be derived by Eq. 5.

$$F_N = \sigma_p \cdot A_T \tag{5}$$

Figure 5a shows the 3D view of the nanomachining process. "1" and "2" denoted in this figure show the previous and latter tip paths, respectively. "3" marked with red line represents the interface between the tip and the sample material. Figure 5b shows the top view of the machining process. "1" and "2" indicated in this figure
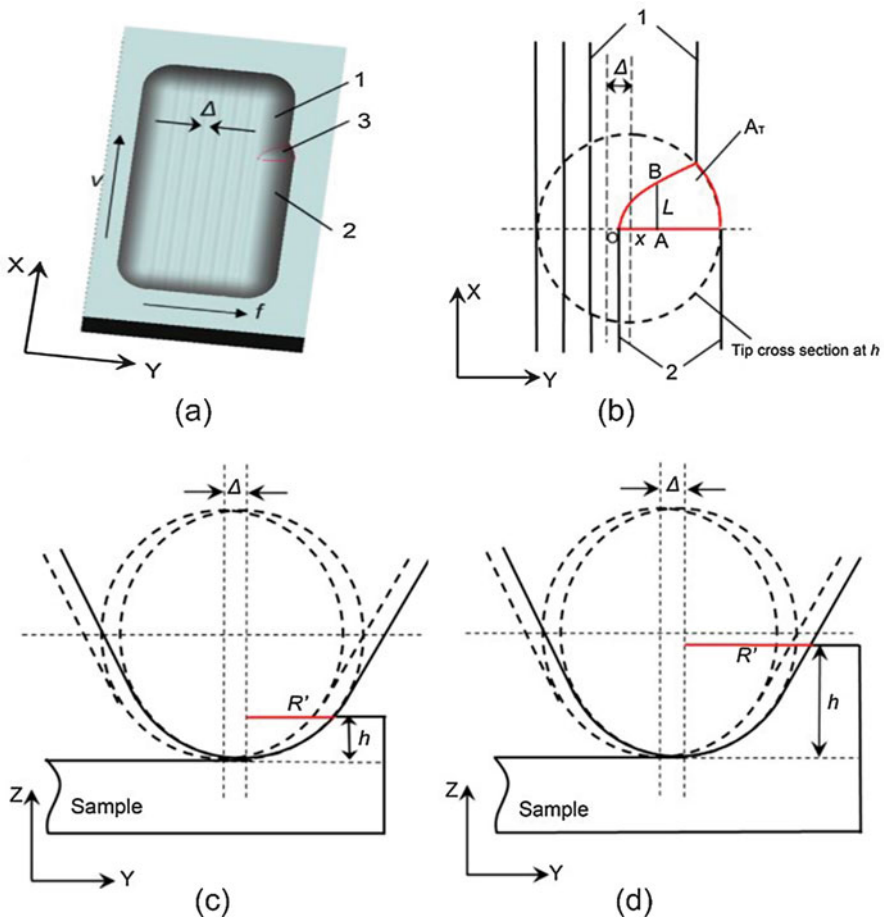

Fig. 5 (**a**) Schematic 3D view of nanomachining processing. (**b**) The top view of the machining process. Front views of the nanostructure fabrication process when $h < h_1$, (**c**) and when $h > h_1$, (**d**) (Reproduced with permission from Geng et al. 2013b)

show the edges of the previous and latter tip paths corresponding to the paths shown in Fig. 5a. The red line in Fig. 5b illustrates the horizontal projection of the interface between the tip and the sample (A_T). In order to study the machined depth, the relationship between A_T and h needed to be considered first. To simplify the calculation, the AFM tip is usually assumed as a cone with a spherical apex (Geng et al. 2013b). Thus, in term of the machined depth, the nanomachining process can be divided into two scenarios: h is larger than the critical depth (h_1) and h is smaller than h_1. The critical depth is the vertical distance from the top of the tip to the connection ring of the cone and the spherical apex, which can be calculated by $R_0(1-\sin\alpha)$. R_0 is the radius of the spherical apex, and α is the tip semi-angle. As shown in Fig. 5b, A_T can be obtained by integrating L with respect to x and adding an arc area, which can be calculated by symbolic computation expressed as (Geng et al. 2013b):

$$A_T = \frac{1}{3}(2R'-\Delta)\cdot\sqrt{(2R'-\Delta)\cdot\Delta} + \frac{1}{2}\arccos\frac{R'-\Delta}{R'}\cdot R'^2 - \frac{1}{2}(R'-\Delta)\sqrt{R'^2-(R'-\Delta)^2} \tag{6}$$

where Δ is the feed value and R' represents the radius of the cross section of the tip at the depth of h, as shown in Fig. 5c and d. In terms of h, R' can be obtained as follows (Geng et al. 2013b):

$$\begin{cases} R' = \sqrt{R_0{}^2-(R_0-h)^2} & h < h_1 \\ R' = (h-R_0(1-\sin\alpha))\cdot\tan\alpha + R_0\cos\alpha & h > h_1 \end{cases} \tag{7}$$

Thus, if nanostructure with a depth is desired to be machined, an applied normal load can be determined from Eqs. 5, 6, and 7 when the feed value is fixed. However, we know that the feed value cannot be extremely small, which can result in the plowing machining state and the bottom of the structure with a relatively large roughness. This is because the edge of the tip is not extremely sharp, which is about 40 nm for the diamond tip (Geng et al. 2013b). Thus, a minimum value of the feed is usually selected as 30 nm. In addition, the feed can also not be chosen a large value. When the feed is larger than a certain value, the tip paths are independent of each other, and the nanochannel cannot be generated (Geng et al. 2013b). Considering the surface quality of machined structure, a maximum feed value is selected as 130 nm. Thus, a moderate feed value should be chosen to guarantee the surface quality of the machined nanostructure.

In our previous study (Geng et al. 2013b), we selected a moderate feed of 60 nm and a reasonable range of machined depth to fabricate sinusoidal nanostructure, as shown in Fig. 6a. Figure 6b shows the corresponding normal load calculated by Eqs. 5, 6, and 7. The scratching speed is set as 10 μm/s, and the width of the structure is 18 μm. Figure 6c shows the AFM image of the machined sinusoidal nanostructure, and Fig. 6d shows the corresponding cross section compared with the desired machined depths. It can be indicated that the machined depth is closed to the
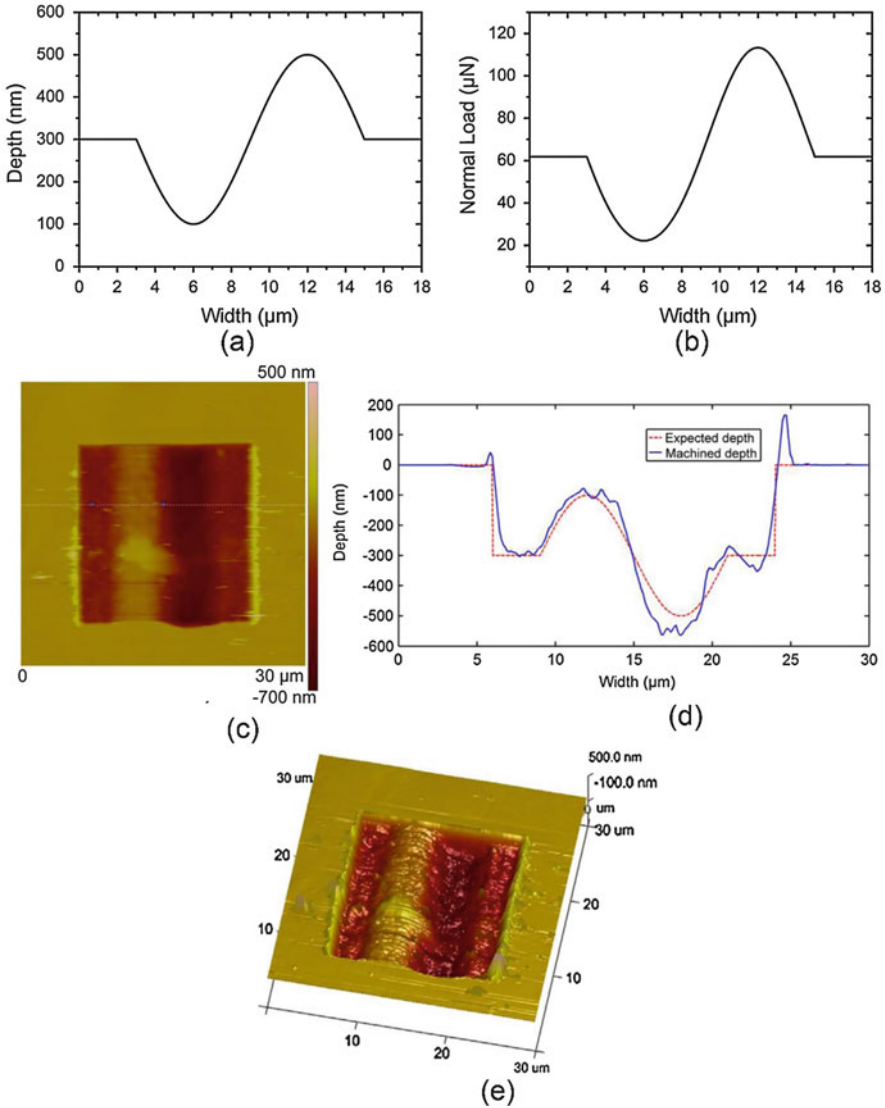
Fig. 6 (**a**) The expected depth of the nanostructure with sinusoidal waveform. (**b**) The corresponding normal load. (**c**) The AFM image of the fabricated nanostructure. (**d**) The corresponding cross-sectional AFM image comparing with the excepted depth. (**e**) 3D AFM image of the machined nanostructure (Reproduced with permission from Geng et al. 2013b)

expected depth, and the sinusoidal nanostructure can be observed clearly from the 3D AFM image of the machined structure, as shown in Fig. 6e. Therefore, the AFM tip-based load-control nanomachining approach has been proven by this work, which can be used to fabricate 3D nanostructure with expected dimensions.

13.3.3 Fabrication 3D Nanostructure by Controlling the Feed Value

As mentioned in Sect. 3.1, the feed value is also a key factor for the machined depth. In the load-control nanomachining method, each point on the nanostructure requires a specific normal load and the accurate location, which may result in relatively time-consuming, while the feed-control approach only needs the feed values for each machined depth and the applied normal load is kept constant. This machining process can be changed into a design of the scratching trajectory. This means the stage can be separated from the AFM system and move to any other AFM system to conduct nanomachining of 3D nanostructure without programming to control the normal load. The AFM is like a tool rest to provide a constant normal force. This approach can be used as a 3D nanostructure machining module in some applications with the advantage of easy operation and high efficiency (Geng et al. 2016c, 2017a). However, the disadvantage of this method is the machined depth along the scratching path should be constant, which may confine the application of this feed-control method.

In this method, the feed is enabled variationally by controlling the scratching trajectory during machining, as shown in Fig. 7a. Figure 7b shows the cross section of the structure with the expected depth, and Fig. 7c illustrates the schematic of the corresponding feed values needed. In particular, the positions A and B shown in Fig. 7b represent the deepest and shallowest points of the structure, respectively. Δ_1 and Δ_2 denoted in Fig. 7c show the feed values required at points A and B, respectively. It can be observed clearly that the depth at point A is larger than that at point B, while Δ_1 is smaller than Δ_2. In addition, the edge-forward is also selected as the feed direction to guarantee the machining quality, and the feed values in the range from 30 nm to 130 nm are chosen.

Comparing with the force-control machining method, this proposed approach should consider the change of the feed value and the depth between the two adjacent scratching paths (Geng et al. 2017a). Figure 8a and b shows the top view of the machining processes with the depth decreasing and increasing, respectively. Figure 8c and d shows the corresponding side view of the machining process. The red and green solid lines in Fig. 8a and b represent the edges of the previous and latter scratching paths, and the dotted cycles denote the horizontal cross section of the AFM tip at the sample surface. Moreover, the blue curved line is the horizontal projection of the interface between the tip and the sample. The red dotted line and green solid line in Fig. 8b represent the vertical cross section of the AFM tip for the previous and latter scratching paths, respectively.

1. As shown in Fig. 8a, when the depth is decreasing, that is, the feed is increasing, it can be observed easily that the radius of the red dotted cycle is larger than that of the green dotted cycle. Similar to the force-control method, the area OCD (S_{OCD}) can be obtained by integrating L with respect to x, as expressed by (Geng et al. 2017a):
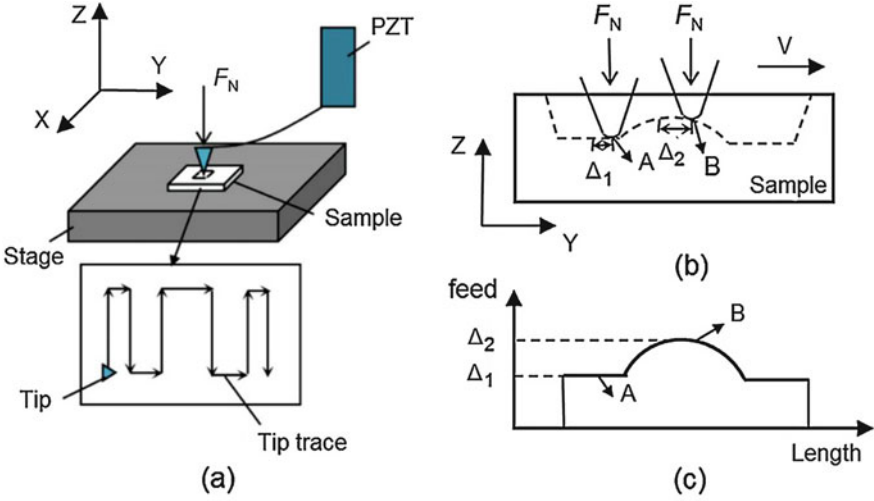
Fig. 7 (**a**) Schematic of AFM-based mechanical machining process using the feed-control approach. (**b**) The dotted line denotes a 3D nanostructure desired to be machined. (**c**) Feed control signal variation during the machining process of the 3D nanostructure shown in (**b**) (Reproduced with permission from Geng et al. 2017a)

$$S_{\text{OCD}} = \int_0^{\sqrt{R_0^2-\left(R_0^2-h_c^2\right)}-\sqrt{R_0^2-\left(R_0-(h_r+\Delta h)^2\right)}} Ld$$
$$x - \int_{\sqrt{R_0^2-\left(R_0^2-h_c^2\right)}-\sqrt{R_0^2-(R_0-(h_r+\Delta h))^2}}^{(R_0\cos\alpha+(h_c+\Delta h-(R_0-R_0\sin\alpha))\tan\alpha)-\sqrt{R_0^2-(R_0-(h_r+\Delta h))^2}} Ld \tag{8}$$
$$x \int_{(R_0\cos\alpha+(h_c+\Delta h-(R_0-R_0\sin\alpha))\tan\alpha)-\sqrt{R_0^2-(R_0-(h_r+\Delta h))^2}}^{R_1'-\sqrt{R_0^2-(R_0-(h_r+\Delta h))^2}} Ldx$$

where Δh is the difference between the two adjacent paths. h_r is the height of the intersection point between the previous and latter paths denoted by point "O" with respect to the deepest point of the current path, as shown in Fig. 8e, which can be calculated by (Geng et al. 2017a):

$$\sqrt{R_0^2 - (R_0 - h_r)^2} + \sqrt{R_0^2 - \left(R_0 - (h_r + \Delta h)\right)^2} = \Delta \tag{9}$$

The area CDE (S_{CDE}) can be calculated by (Geng et al. 2017a):

$$S_{\text{CDE}} = \frac{1}{2}\arccos\left(\frac{R_1' - \Delta}{R_2'}\right) \cdot R_2'^2 - \frac{1}{2}(R_1' - \Delta)\sqrt{R_2'^2 - (R_1' - \Delta)^2} \tag{10}$$

where R_1' and R_2' are the radii of the horizontal cross section of the AFM tip at the sample surface for the previous and latter paths, which can be expressed by (Geng et al. 2017a):
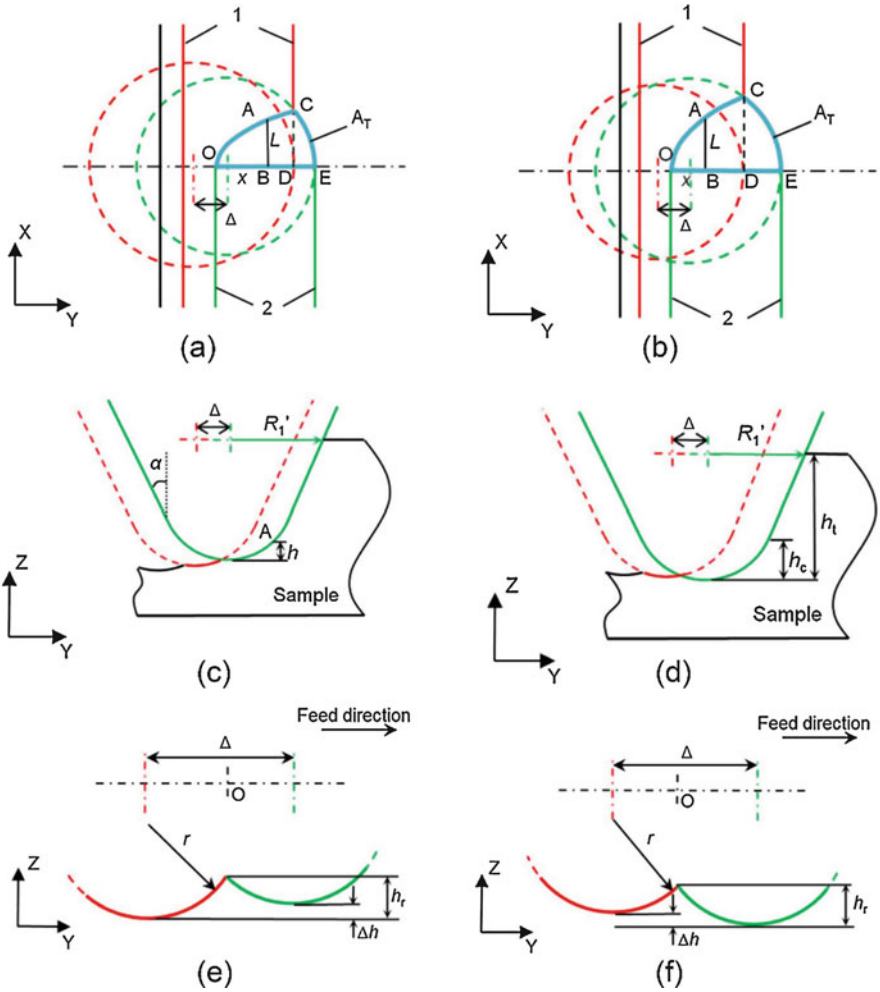
Fig. 8 Top views of the machining process when the feed is increasing (**a**) and when the feed is decreasing (**b**). Front views of the machining process when the feed is increasing (**c**) and when the feed is decreasing (**d**). Side views of the 3D-MNS fabrication process. Feed increasing (**e**) and feed decreasing (**f**) (Reproduced with permission from Geng et al. 2017a)

$$\begin{cases} R_1' = R_0 \cos\alpha + (h + \Delta h - (R_0 - R_0 \sin\alpha)) \tan\alpha \\ R_2' = R_0 \cos\alpha + (h - (R_0 - R_0 \sin\alpha)) \tan\alpha \end{cases} \tag{11}$$

Thus, A_T can be obtained by the sum of S_{OCD} and S_{CDE}.

2. When the depth is increasing and the feed values decreases, the radius of the green dotted cycle is larger than that of the red one, as shown in Fig. 8b. In this case, S_{OCD} can be obtained by (Geng et al. 2017a):

$$
S_{\text{OCD}} = \int_0^x \frac{\sqrt{R_0{}^2 - \left(R_0{}^2 - (h_c - \Delta h)^2\right)} - \sqrt{R_0{}^2 - \left(R_0 - (h_r - \Delta h)\right)^2}}{L} \mathrm{d}
$$
$$
x - \int_x^{R_1'} \frac{(R_0 \cos \alpha + (h_c + \Delta h - (R_0 - R_0 \sin \alpha)) \tan \alpha) - \sqrt{R_0{}^2 - (R_0 - (h_r - \Delta h))^2}}{\sqrt{R_0{}^2 - \left(R_0{}^2 - (h_c - \Delta h)^2\right)} - \sqrt{R_0{}^2 - (R_0 - (h_r - \Delta h))^2}} L \mathrm{d}
$$
$$
\frac{R_1' - \sqrt{R_0{}^2 - (R_0 - (h_r - \Delta h))^2}}{(R_0 \cos \alpha + (h_c - (R_0 - R_0 \sin \alpha)) \tan \alpha) - \sqrt{R_0{}^2 - (R_0 - (h_r - \Delta h))^2}} L \mathrm{d}x \tag{12}
$$

The relationship between h_r and Δ is now changed to (Geng et al. 2017a):

$$
\sqrt{R_0{}^2 - (R_0 - h_r)^2} + \sqrt{R_0{}^2 - (R_0 - (h_r - \Delta h)^2} = \Delta \tag{13}
$$

The area CDE (S_{CDE}) can also be calculated by Eq. 10 given for the previous scenario. However, in this case, R_1' and R_2' should be changed to (Geng et al. 2017a):

$$
\begin{cases} R_1' = R_0 \cos \alpha + (h - \Delta h - (R_0 - R_0 \sin \alpha)) \tan \alpha \\ R_2' = R_0 \cos \alpha + (h - (R_0 - R_0 \sin \alpha)) \tan \alpha \end{cases} \tag{14}
$$

Thus, A_T can also be obtained by summing S_{OCD} and S_{CDE}.

In our previous study (Geng et al. 2017a), we found that the slope values of the nanostructures can only be selected in the range from $-12°$ to $+12°$ to guarantee a machining error within 10% when conducting machining process on the single-crystal copper surface with the (110) crystallographic plane. The sample surface was polished by the manufacturer, and the roughness (R_a) is less than 5 nm, which is measured by the tapping mode of the AFM system. The possible reasons for the selection range of the slope value have been given as follows. First, the adjacent scratching paths should not affect each other during the machining process to guarantee the machining quality. Thus, applying Eqs. 13 and 14, an inequation can be derived as follows (Geng et al. 2017a):

$$
\frac{\Delta h}{\Delta} < \tan \left(\frac{\pi}{2} - \alpha \right) \tag{14}
$$

The ratio of Δh and Δ is defined as the slope of the nanostructure. The AFM tip used in our previous study (Geng et al. 2017a) is 60° based on the SEM image. Thus, it can be found from Eq. 14 that the slope of the expected nanostructure should be less than 30°. In addition, the relationship between the feed value and the machined depth is usually obtained by the machining experiments of the cavities with planar floor surfaces, for the cavities with planar floor surfaces are machined with the constant-feed method and the point "O" shown in Fig. 8a and b should be in the middle of the green and red dotted cycles. However, it can be observed for Eq. 9 that the point "O" is closed to the center of the green dotted cycle for the latter path in the case of the machined depth decreasing, as shown in Fig. 8e, while the point "O" is closed to the center of the red dotted cycle for the previous path in the case of the machined depth increasing, as shown in Fig. 8f. Thus, the length of the integral for

A_T (OE shown in Fig. 8a and b is smaller in the case of depth decreasing and larger in the condition of depth increasing, compared with the situation of machining the planar floor surface. Moreover, it can be found from Fig. 8a and b that L is smaller in the case of the depth decreasing and larger in the condition of depth increasing compared with the situation of machining the planar floor surface. Thus, from Eqs. 8, 10, and 12, it can be indicated that the sum of S_{OCD} and S_{CDE}, that is, A_T, is smaller in the case of depth decreasing and larger in the condition of depth increasing. With the same normal load, if A_T is smaller, the AFM tip should be penetrated deeper in the case of the depth decreasing. This can result in the slope of the structure smaller than the setting value. While, if A_T becomes larger, the depth penetrated by the AFM tip should be shallower in the condition of the depth increasing. This can also cause the reduce of the slope of the structure. Therefore, by utilizing the relationship between the feed values and depth obtained by machining the cavities with planar floor surfaces to fabricate 3D nanostructure, the obtained slope of the structure should be less than that of the expected value. Moreover, the larger slope is chosen, the difference between the achieved and desired values is larger. Thus, to guarantee the machining error less than 10%, the slope in the range from $-12°$ to $+12°$ can be selected.

Based on the above discussion, typical sinusoidal waveforms nanostructures were fabricated to demonstrate the feasibility of the feed-control nanomachining approach in our previous study (Geng et al. 2017a). The period of the desired sinusoidal waveform nanostructures (T) should satisfy the inequation as described below:

$$T \geq \frac{2\pi a_s}{\tan(\theta_c)} \tag{14}$$

where a_s represents the amplitude of the structure, and θ_c is the critical value of the slope, which should be $12°$. If the amplitude is selected as 80 nm, the period (T) should be larger than or equal to 2.4 µm. When the amplitude is chosen as 125 nm, the minimum value of the period can be calculated as 3.74 µm. Thus, we chose two group machining parameters to conduct the machining processes of the typical sinusoidal waveform nanostructures. The first one is machining with the normal load of 102.4 µN, the amplitude of 80 nm, the base depth of 240 nm, and the period of 2.4 µm. The second one is fabricating with the normal load of 145.1 µN, the amplitude of 125 nm, the base depth of 275 nm, and the period of 4 µm. The 2D and 3D AFM images of the two sinusoidal waveform nanostructures are shown in Fig. 9a and b, respectively. From the cross sections of the machined nanostructure, it can be indicated that the results are consistent with the desired values. This can prove the feasibility of the feed-control approach to fabricate 3D nanostructure with expected dimensions.

13.4 Fabrication of 3D Nanostructure by Stick-Slip Process

Comparing with the metal material, the polymer can hardly be removed by the AFM tip with the formation of the chips. This is because the polymer material is usually accumulated on the sides of the groove to generate material pileups during the
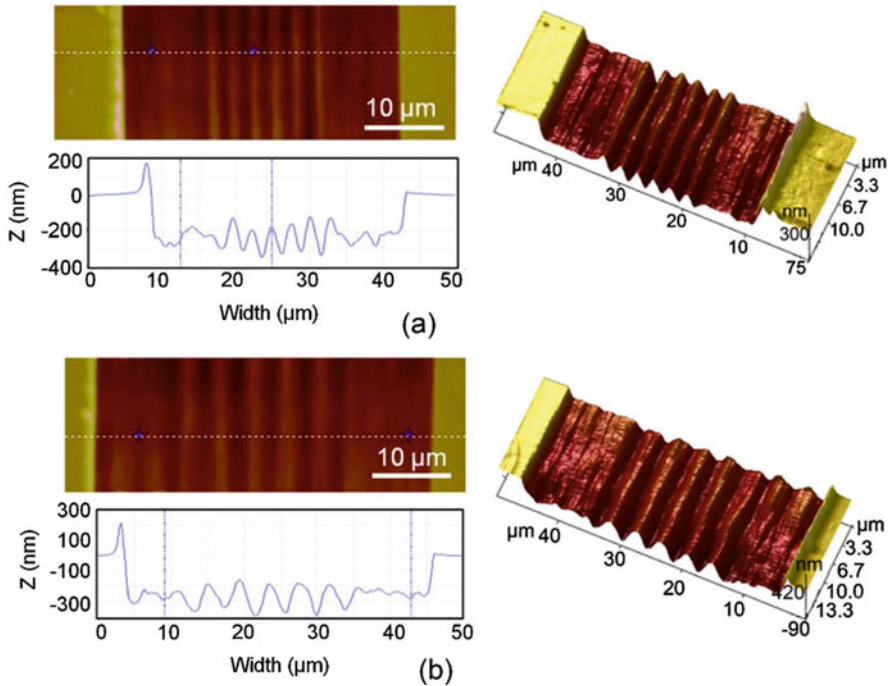
Fig. 9 AFM images of the machined nanochannels with desired sinusoidal waveforms nano-structures: (**a**) the period of 2.4 μm and (**b**) the period of 4 μm (Reproduced with permission from Geng et al. 2017a)

scratching process. Nano-periodic pattern was first found during investigating nano-tribological behavior of the polymer material with the AFM tip (Aoike et al. 2001). This ripple-type nanostructure is perpendicular to the scratching direction. However, the ripple-type nanostructure was always formed by more than 10 times of reciprocal scanning on the sample surface with an extremely small normal load (several nano-newton) (Aoike et al. 2001), which is not suitable to be considered as a novel nanofabrication method due to the time-consuming of the process and uncertainty of the dimensions of the obtained structures. Thus, fabrication the ripple-type nanostructure with only one scratching process is needed. Moreover, the investigation of the approach to control the period and amplitude of the ripple-type nano-structure is also required. D'Acunto et al. (2007) proved that the ripple-type nanostructure can be formed with only one scanning process on PCL and PET polymer film surfaces by using a relatively small normal load (several nano-newton). However, the amplitude is very small and uncontrollable. Thus, in our previous study (Sun et al. 2012), we considered enlarging the applied normal load (tens of micro-newton) to increase the amplitude of the ripple-type structure and controlling the period and amplitude for one-scan machining process. The formation mecha-nisms for the ripple-type nanostructure are usually explained as Schallamach waves,

stick-slip process, fracture mechanisms, and erosion-diffusion process (Aoike et al. 2001; Yang et al. 2013; Dinelli et al. 2005; Surtchev et al. 2005; Elkaakour et al. 1994), which are different from the material removal mechanism in the machining process of metal material. Thus, the influence of the scratching parameters on the machining results is also different. Similarly, the scratching trajectory and feed direction are also needed to be studied first.

Figure 10 shows the three typical machining trajectories in the scratching process on the polymer surface, which are zigzag, rectangular, and line-scratch types. For the zigzag tip trace, the AFM tip is controlled by the AFM scanner along the X and Y directions to achieve the tip trace, as shown in Fig. 10a and b, which is the same with the scanning process of the AFM system. The rectangular trajectory is obtained by the relative motion between the tip and the sample along the X and Y directions, as shown in Fig. 10c and d. The position of the AFM tip is kept constant in the horizontal plane, and the sample is driven by the high precision. The vertical position of the AFM tip can be adjusted by the AFM scanner in Z direction to keep the normal load constant during the machining process. As shown in Fig. 10e and f, the movement of the sample is also controlled by the high-precision stage, and the position of the AFM tip is also kept constant in the horizontal plane. However, after the tip accomplishing one scratch, the sample is controlled to conduct the vertical downward motion by the high-precision stage. This can cause the tip separating with the sample surface due to the limitation of the AFM scanner in Z direction. This operation is similar as the tip lifting up, which is denoted by BB' shown in Fig. 10f. Then, the sample is controlled to return the initial point of the scratch, denoted by B'A' in Fig. 10f. After the sample reaching point A', it moves upward to contact with the AFM tip again. This step is similar with the approaching process. A feed is then conducted toward the positive direction of X axis to accomplish one scratching cycle. In our pervious study (Yan et al. 2012), experimental tests were carried out to compare these three scratching trajectories.

Figure 11 shows the AFM images of the ripple-type nanostructures machined with the zigzag and rectangular trajectories, respectively. The machining ranges are 10 μm × 10 μm and 8 μm × 8 μm, respectively. The feed is set as 10 nm, and the normal load is selected as 5.2 μN. The feed direction is chosen as the edge-forward. The dislocation phenomenon of the cross sections of the AFM image at three different points can be observed easily from Fig. 11b, which is machined with the zigzag trajectory, while the cross sections of the AFM image are consistent with each other when machining with the rectangular trajectory, as shown in Fig. 11d. The possible reason can be given as follows. For the zigzag trajectory, the feed in one scratching cycle is not kept constant, which is smallest at the beginning and largest at the end of the scratching cycle. Moreover, due to the reciprocating motion of the AFM tip, the beginning and the end points are alternant for the adjacent scratching cycles. Here, we utilize the stick-slip and crack formation processes to explain the machining results (Elkaakour et al. 1994). When scratching on the surface of the polymer material, a material pileup can be generated, and a lateral force can thus be applied on the tip apex. This lateral force (F_t) can be expressed by Eq. 15, which is resulted from the elastic energy stored in the substrate (Elkaakour et al. 1994).
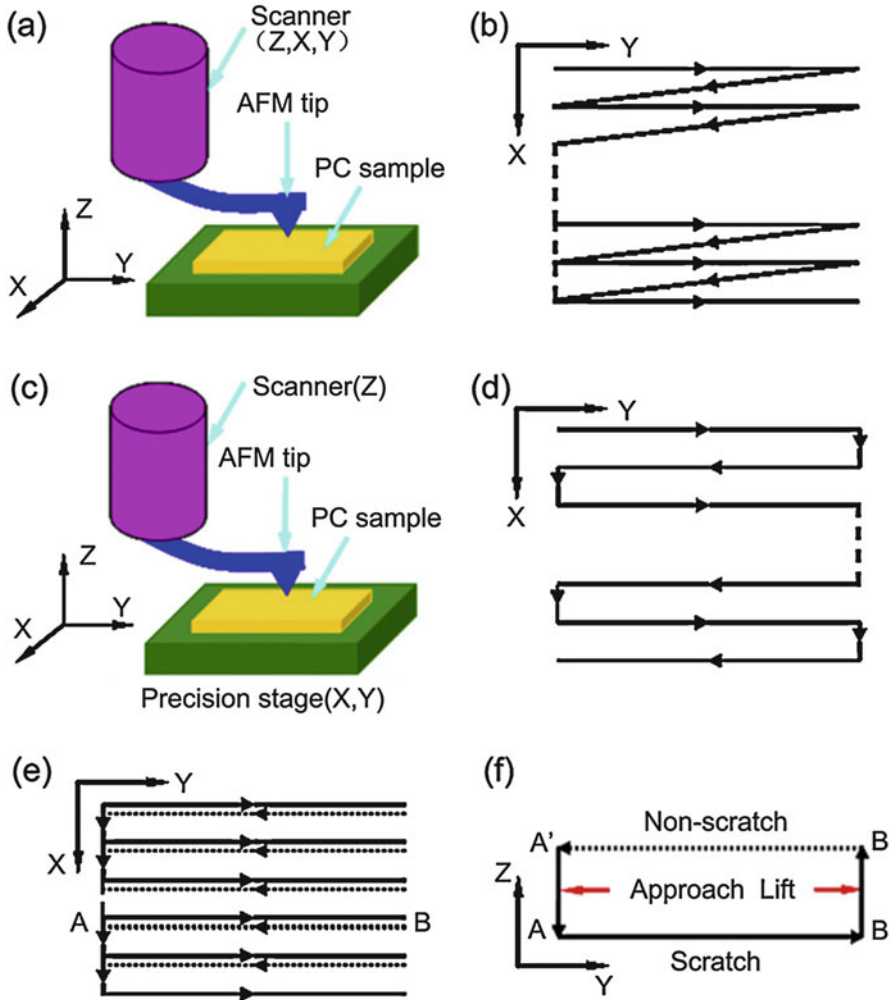
Fig. 10 Schematic illustration of the machining systems and the corresponding tip traces. (**a**) The AFM system, (**b**) the zigzag trajectory, (**c**) the modified AFM system, (**d**) the rectangular trace, (**e**) the line-scratch trace of the modified AFM system, and (**f**) the tip's motion in each line of (e) (Reproduced with permission from Yan et al. 2012)

$$F_t = \frac{Eah}{2} \frac{\tau}{L} \qquad (15)$$

where E, a, and h are Young's modulus of the substrate, the radius of the tip-sample contact area, and the machined depth, respectively. L and τ represent the length of the internal defect and strain yielded, respectively (Elkaakour et al. 1994). When this lateral force (F_t) reaches a critical value (F_{tc}), the AFM tip can slide over the material pileup instead of pushing the polymer material to form a groove (Elkaakour et al.
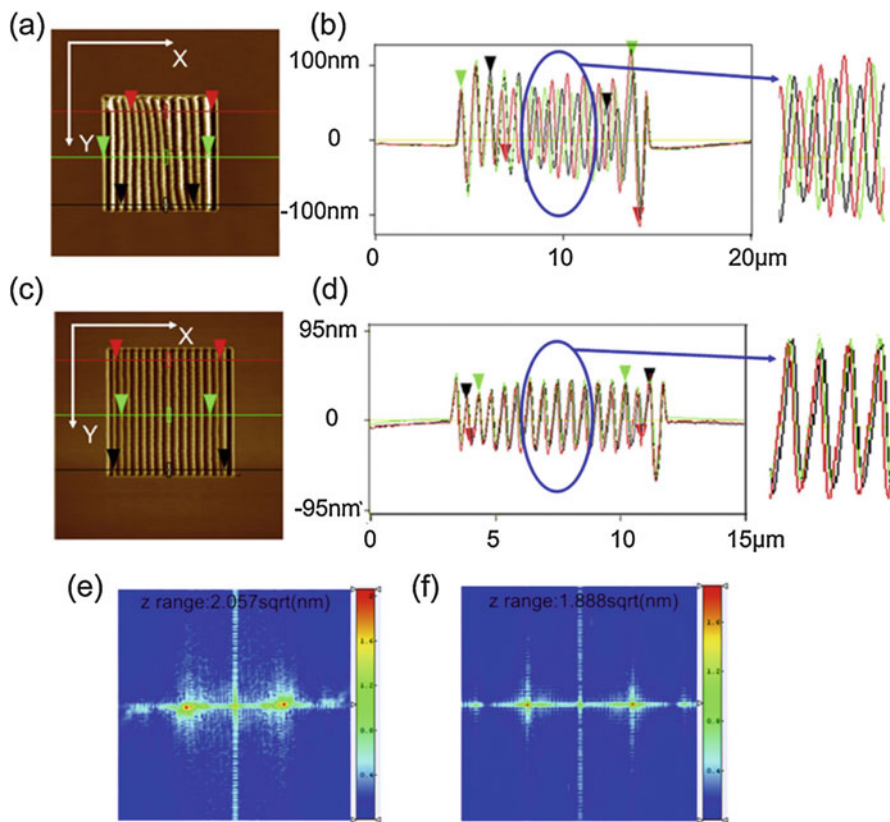
Fig. 11 The morphologies and the corresponding FFT of the sample surface for once scratching with the AFM system and the modified AFM system, respectively (Reproduced with permission from Yan et al. 2012)

1994). This critical force value (F_{tc}) is related to the friction coefficient, applied normal load, radius of the AFM tip, and surface energy term (Elkaakour et al. 1994). If the feed is changing all the time during the machining process, that is, the radius of the tip-sample contact area and machined depth changing, the lateral force (F_t) is thus changed. The scratching length to form one peak of the ripple structure is also changing in one cycle, which may cause the dislocation of the cross sections. This may also result in the inconsistent amplitude of the ripple structure, as shown in Fig. 11b. For the rectangular trajectory, the feed value is kept constant in one scratching cycle. The lateral force (F_t) applied on the apex of the tip is changeless during the machining process. Thus, the period and amplitude of the ripple nanostructure is stable. It can be indicated that the rectangular trajectory is more suitable than the zigzag trace considering the machining quality of the ripple-type nanostructure. The AFM image was also analyzed in our previous study using the means of the fast Fourier transform (FFT) function, as shown in Fig. 11e and f (Yan et al. 2012). It

can be observed that the structure machined with the rectangular trajectory shows a better periodical property than that machined with the zigzag trajectory, which agrees well with the above discussion.

To study the difference between the rectangular and the line-scratch trajectories, a small feed of 10 nm is selected. When scratching with the rectangular trace, the machining range is chosen as 8 μm × 8 μm, and the normal load is set as 2.5 μN. For the line-scratch trajectory, the machining range is select as 10 μm × 10 μm, and the normal load is chosen as 2 μN. Figure 12a and b shows the AFM images of the structures machined with the rectangular and the line-scratch trajectories, respectively. It can be observed that only one groove and ridge, rather than ripple-type
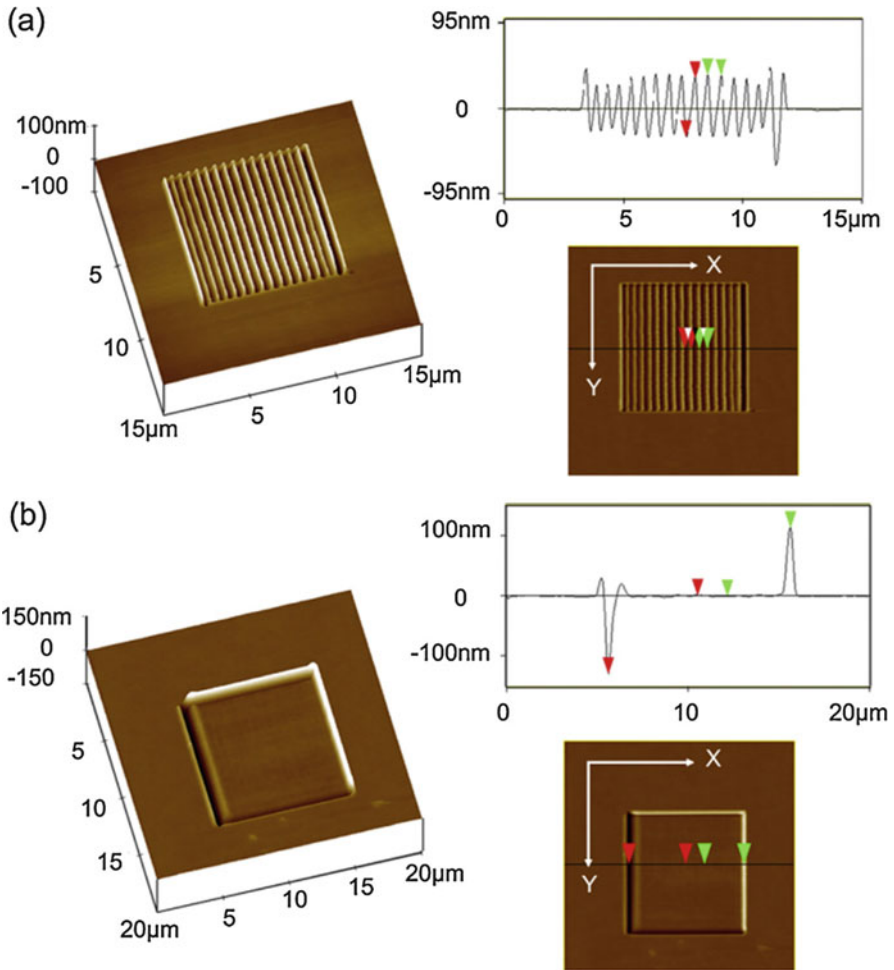

Fig. 12 The morphologies of the scratched sample surface with the feed of 10 nm: (a) rectangular trajectory and (b) line-scratch trajectory (Reproduced with permission from Yan et al. 2012)

nanostructure, can be formed when machining with the line-scratch trajectory. The reason for this phenomenon is attributed to the different scratching paths for the rectangular and the line-scratch trajectories. As shown in Fig. 12b, the left side of the cross section of the AFM image is the beginning point of the scratching process. A groove with a relatively large depth can be found at the beginning point in this case. Figure 13a–d shows the schematic of the front view of the scratching process with the line-scratch trajectory (Yan et al. 2017). As shown in Fig. 13a, the AFM tip penetrates into the sample surface with a preset normal load. After the tip scratching with a small length, one side of the tip is separated from the sample. Thus, the tip is pressed into the sample deeper to balance the normal load, and the height of the material pileup becomes larger due to the increase of the machined depth, as shown in Fig. 12b. With the increase of the material accumulation on the front of the main cutting surface of the AFM tip, the tip should move upward to keep the efficient contact area between the tip and the sample constant, as shown in Fig. 12c. The lateral force (F_t) applied on the tip apex generated by the material pileup is not large enough to reach the critical force value (F_{tc}). Thus, the tip cannot slide over the material pileup. Instead, the material pileup is pushed to the end point by the AFM tip, as shown in Fig. 12d, which is formed the ridge structure at the right side of the structure observed in the cross section of the AFM image. For the rectangular trajectory, the AFM tip is carried out a reciprocating motion. Some material can be pushed to the beginning side of the structure. Thus, the height of the material accumulated at the beginning side of the structure is relatively larger than that machining with the line-scratch trajectory. Figure 13e and f shows the schematic of the front view of the scratching process with the rectangular trajectory (Yan et al. 2017). Due to the large material pileup at the beginning point, the depth penetrated by the AFM tip is smaller, as shown in Fig. 13e. As a result, the height of the material accumulated on the front of the main cutting surface of the AFM tip should be also
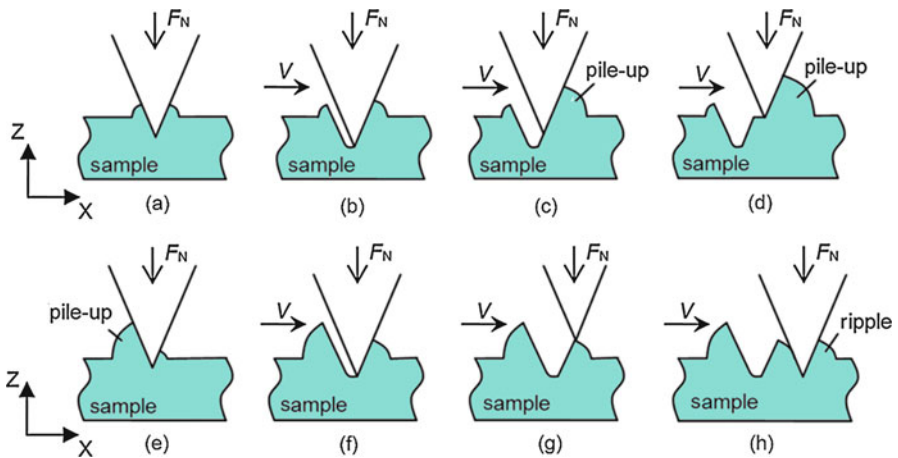

Fig. 13 Formation process of the ripple-type nanostructure: (**a**–**d**) scratching with the line-scratch trajectory and (**e**–**h**) scratching with rectangular trajectory

smaller, as shown in Fig. 13f. Both the substrate material and the pileup take part in contacting with the AFM tip. In this case, the lateral force (F_t) may be large enough to reach the critical force value (F_{tc}) to slide over the pileup, as shown in Fig. 13g. The AFM tip then presses into the sample surface again to form another hump, as shown in Fig. 13h. Therefore, it can be indicated that the scratching trajectory has a large influence on the formation of the ripple-type nanostructure, and the rectangular trajectory is the most suitable for the machining of ripple-type nanostructure.

We also investigated the influence of the feed direction on the formation of the ripple-type nanostructure (Yan et al. 2014). The edge-forward, an included angle of 45° and 90° with the edge-forward feed directions were selected, which are named as 0°, 45°, and 90°, respectively. The zigzag trajectory was chosen, the machining area was set as 15 μm × 15 μm, and the scratching velocity was 30 μm/s. Figure 14a shows the machining parameters selected for the scratching tests. Figure 14b–d shows the relationship between the period of the ripple-type nanostructure, applied normal load, and feed value. It can be observed that the feed direction has a large influence on the formation of the ripple-type nanostructure. This reason can be explained as follows. Different cutting angles for various feed directions affect the contact area between the tip and the sample material. In addition, the deformation of the tip cantilever is also changed with different scratching directions, which affects
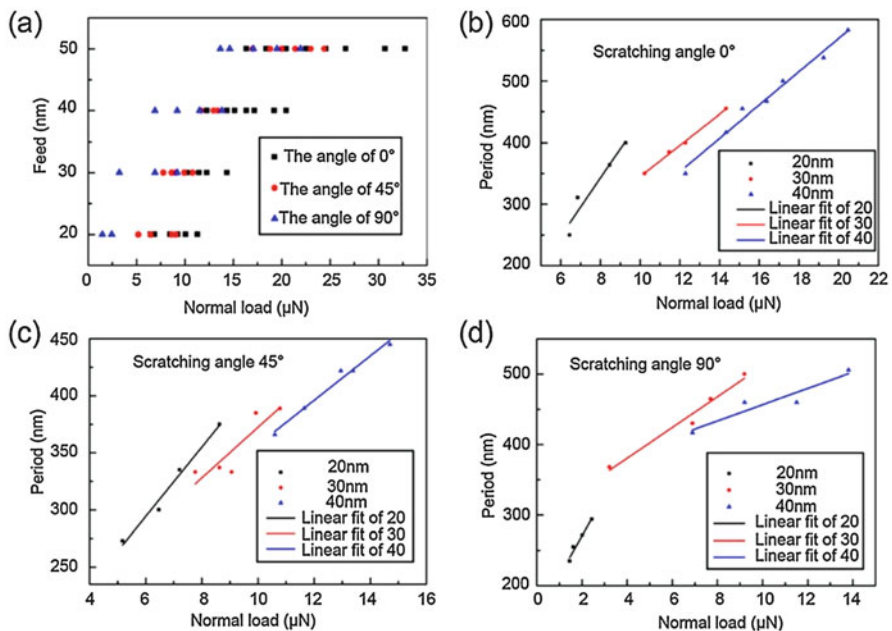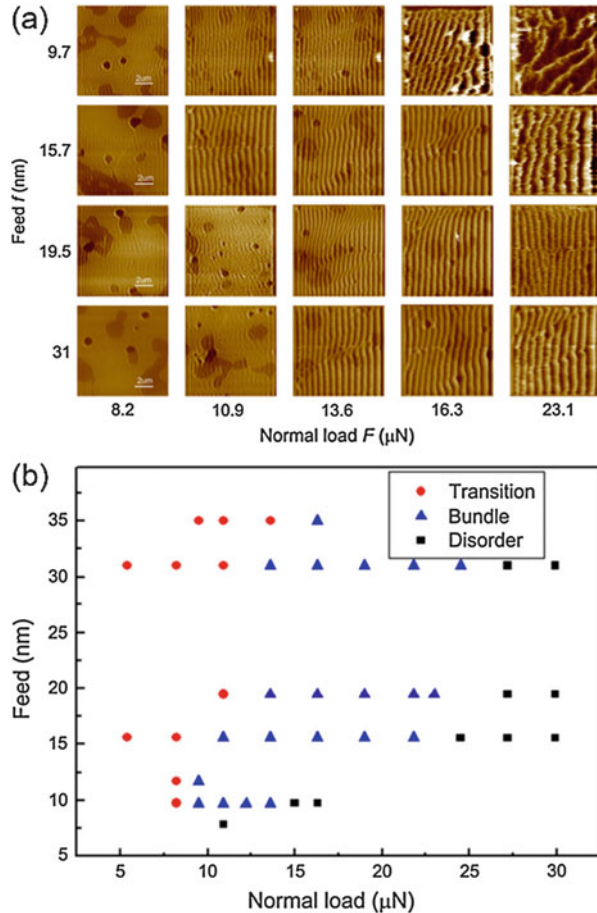

Fig. 14 The relationship between the feed, normal load, and ripple formation. Effects of feed and normal load on (**a**) ripple formation and (**b–d**) the period of ripples for different scratching angles (Reproduced with permission from Yan et al. 2014)

the actual normal load applied on the sample surface (Yan et al. 2014). The tip-sample contact area and the actual normal load can affect the lateral force (F_t) applied on the tip apex and the critical force value (F_{tc}), which can thus result in the changing of the period and amplitude of the machined ripple-type nanostructure. Based on the results shown in Fig. 14, it can be indicated that the period scope for the ripple-type nanostructure follows the order $0° > 90° > 45°$ for the three feed directions.

In order to fabricate ripple-type nanostructure with controllable period and amplitude, the influence of the machining parameters, including the applied normal load and the feed value, on the results should also be studied. In our previous (Sun et al. 2012), five normal loads of 10.9 μN, 13.6 μN, 16.3 μN, and 23.1 μN were selected, and four feed values of 9.7 nm, 15.7 nm, 19.5 nm, and 31 nm were chosen to conduct scratching tests on PC sample surface. The rectangular trajectory and edge-forward feed direction were employed. Figure 15 shows the AFM images of the obtained nanostructures and the feasibility analysis of the selected machining parameters, respectively. It can be observed from Fig. 15a that the ripple nanostructure cannot be formed when scratching with small normal loads and relatively large feed values, such as the normal loads of 8.2 μN and 10.9 μN, and the feed values of 19.5 nm and 31 nm. As mentioned above, the normal force and the feed value can affect the lateral force applied on the tip apex (F_t) and the critical force value (F_{tc}). If the F_t cannot reach the critical force value F_{tc}, the ripple-type nanostructure cannot be formed. When scratching with a small normal load and large feed value, the machined depth is relatively small, which will cause a relatively small lateral force (F_t). Thus, in these cases, the lateral force may be not larger enough for the AFM tip sliding over the pileup to form the ripple-type structure. It can also be found from Fig. 15a that the deformation of the ripple-type nanostructure occurs when scratching with a relatively large normal load, such as 16.3 μN and 23.1 μN. In particular, the nanostructure becomes disordered with a small feed value, such as 9.7 nm. This phenomenon can be explained as follows. When the normal load is relatively large and the feed is relatively small, the latter scratching path can affect the pervious scratching path a lot, which results in the formation of the disorder nanostructure, rather than the ripple-type nanostructure. In order to obtain the influence of the normal and feed value more clearly, the feasibility analysis was conducted (Sun et al. 2012). The result of the feasibility analysis is shown in Fig. 15b. We defined the "Transition" state as the indistinct structure, such as the morphology obtained with the normal load of 8.2 μN and the feed of 9.7 nm. The "Bundle" state means the formation of the regular ripple-type nanostructure. The "Disorder" state indicates the generation of the disordered nanostructure. From Fig. 15b, the range of the normal load and the feed value for generation ripple-type nanostructure can be obtained, which can give an instruction on the machining parameters selection for the fabrication of the ripple-type nanostructure with good quality (Sun et al. 2012).

Figure 16a shows the relationship between the feed value, the period, and the amplitude of the ripple-type nanostructure. It can be observed that both the period and the amplitude are increasing slightly with the feed going up when scratching

Fig. 15 (**a**) AFM image of the machined nanostructure with different normal loads and feeds. (**b**) Effects of the feed and the normal load on formation states of ripple structures (Reproduced with permission from Sun et al. 2012)


with the normal load of 13.6 μN and 19.0 μN. Figure 16b shows the relationship between the normal load, the period, and the amplitude of the ripple-type nanostructure. It can be found that both the period and the amplitude increase dramatically with the normal load going up when scratching with the feed of 19.5 nm. Therefore, we can conclude that the normal load has a greater influence on the machining outcomes than the feed value.

13.5   Fabrication of 3D Nanostructure by Combining the Material Accumulation and the Machined Nanogroove

Recently, an easy and novel approach to fabrication 3D nanostructure was proposed in our pervious study (He et al. 2018). As shown in Fig. 17a, we knew that a large pileup can be formed when scratching on the polymer material with an AFM tip. The proposed method is just considered simply combining the material pileup and the

Fig. 16 (**a**) Relationships between the period, the height amplitude, and the feed value. (**b**) Relationships between the period, the amplitude, and the normal load (Reproduced with permission from Sun et al. 2012)
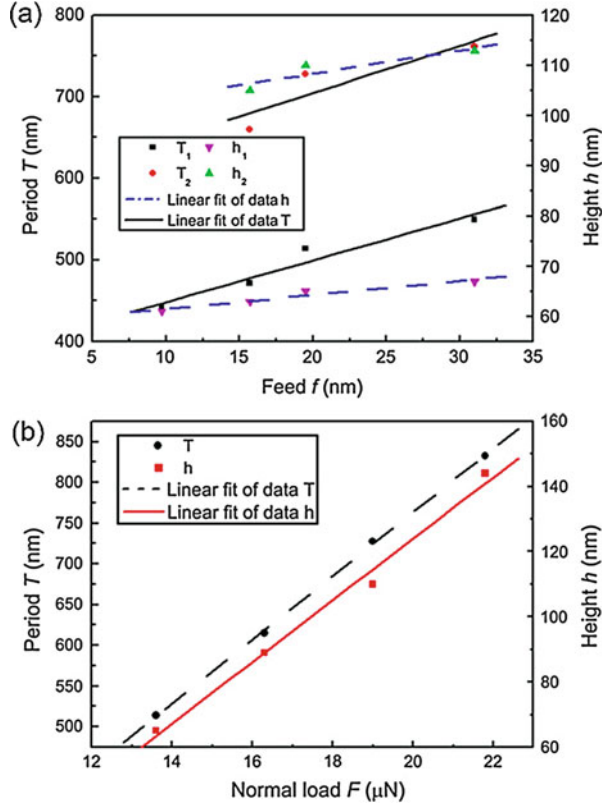
machined groove to form a 3D nanostructure by controlling the separation distance between parallel adjacent scratching paths. Comparing these methods mentioned above, this approach shows the properties of high efficiency, easy operation, and high feasibility for various applications. Considering the sample material, the tapping mode and silicon AFM tip are employed. Due to the geometrical asymmetry of the silicon tip, the scratching direction has a large influence on the profile of the machined groove, as shown in Fig. 17b. The sample material is a poly(methyl methacrylate) (PMMA) thin film. Figure 18a shows the AFM image of the typical groove machined with sideface-forward scratching direction (denoted 90° in Fig. 17a), in which the scratching direction is perpendicular to the tip cantilever. Figure 18b presents the AFM image of the typical groove machined with edge-forward scratching direction (denoted 0° in Fig. 17a), in which the scratching direction is parallel to the tip cantilever. It can be observed that the material is only accumulated on one side of the groove when scratching with sideface-forward scratching direction, while, for the edge-forward scratching direction, the material pileup can be found on both sides of the groove. The period is defined as the total width of the groove and pileup, as shown in Fig. 18. The height and the depth can be measured by the cross section of the AFM image.
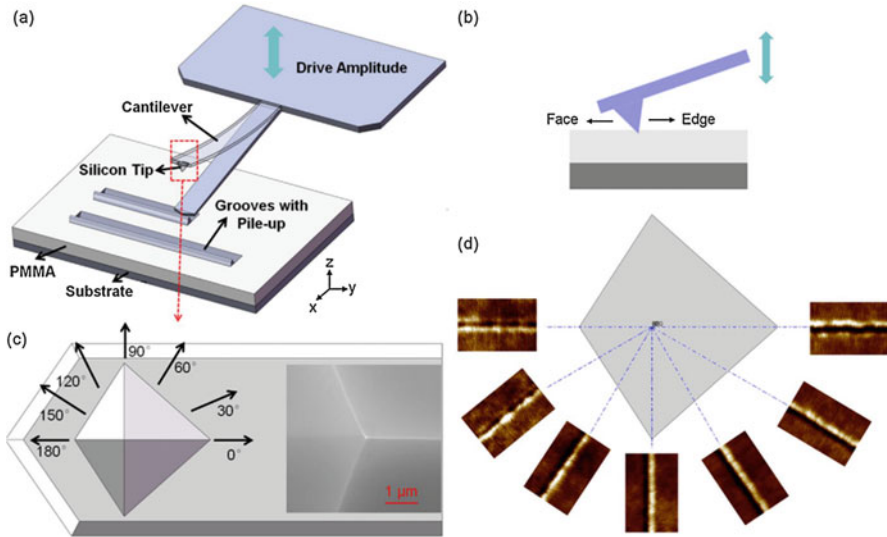
Fig. 17 (**a**) Schematic of grooves with pileup fabrication on a PMMA thin film using tapping mode. (**b**) Edge- and face-forward writing directions. (**c**) Geometry of a silicon tip. (**d**) AFM images of grooves obtained from different scanning directions (Reproduced with permission from He et al. 2018)

We selected sideface-forward scratching direction to conduct the machining process of the 3D nanostructure because the pileup only exists on one side of the groove and the other side can be connected with the material pileup of adjacent groove. The separation distance between parallel adjacent scratching paths can be chosen as the corresponding period of the groove. Figure 19 shows the machined 3D nanostructure with the wavelength of 30 nm and 40 nm. It can be found that the machining quality of the structure is good. The wavelength of the machined structure is determined by the period of the groove, and the amplitude is controlled by the machined depth of the groove. From Fig. 19, it can be indicated that this proposed method is feasible to fabricate 3D nanostructure.

13.6 Summary and Outlook

The AFM tip-based nanomechanical machining method shows advantages of nano-scale machining accuracy, wide range of applicable materials, atmospheric environment requirement, and low cost. In this chapter, we introduce several approaches based on this technique to fabricate 3D nanostructure with desired dimensions.

1. The force-control method is the most intuitive way to fabricate nanostructures with fluctuant machined depth. The feed value is kept constant during the whole scratching process. The relationship between the machined depth, applied normal,
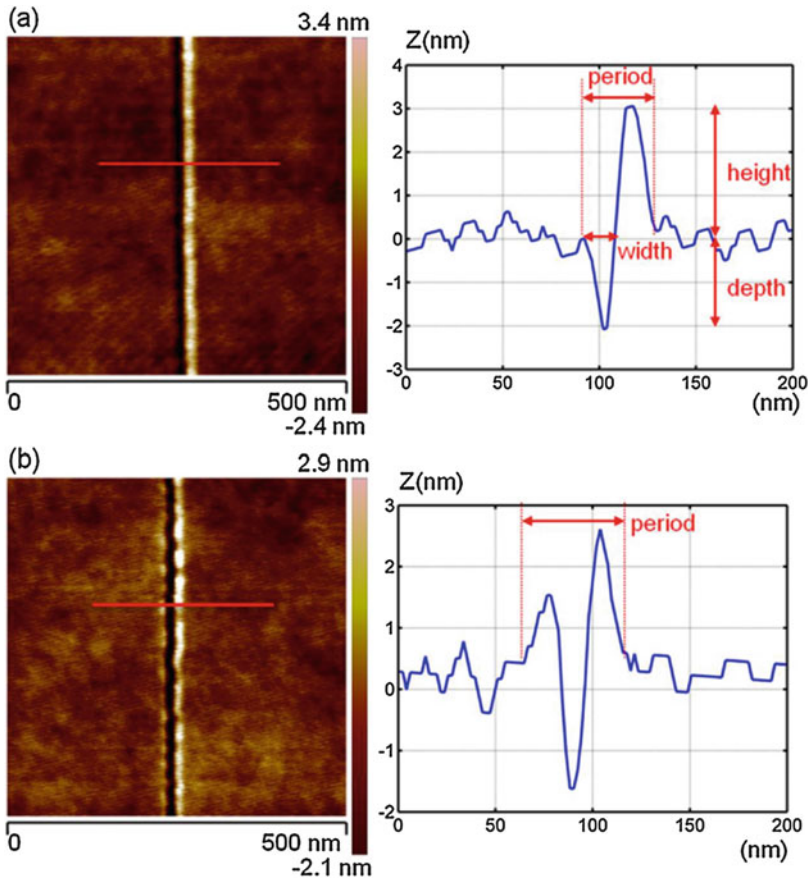
Fig. 18 AFM images and cross sections of grooves fabricated with (**a**) pileup accumulated at 90° along one side and (**b**) pileup accumulated at 0° along both sides (Reproduced with permission from He et al. 2018)

and feed value can be obtained by calculation of the tip-sample contact area. However, in the load-control method, each point on the nanostructure requires a specific normal load and the accurate location. This may result in relatively time-consuming.

2. For the feed-control approach, only the feed values for each machined depth is needed. The applied normal load is kept constant. This machining process can be changed into a design of the scratching trajectory, which can improve the machining efficiency.

3. 3D ripple-type nanostructure can be fabricated on the surface of the polymer material by the stick-slip process. This ripple-type nanostructure is perpendicular to the scratching direction. The applied normal load, tip-sample contact area, geometrical shape of the tip, and deformation of the tip cantilever have a large
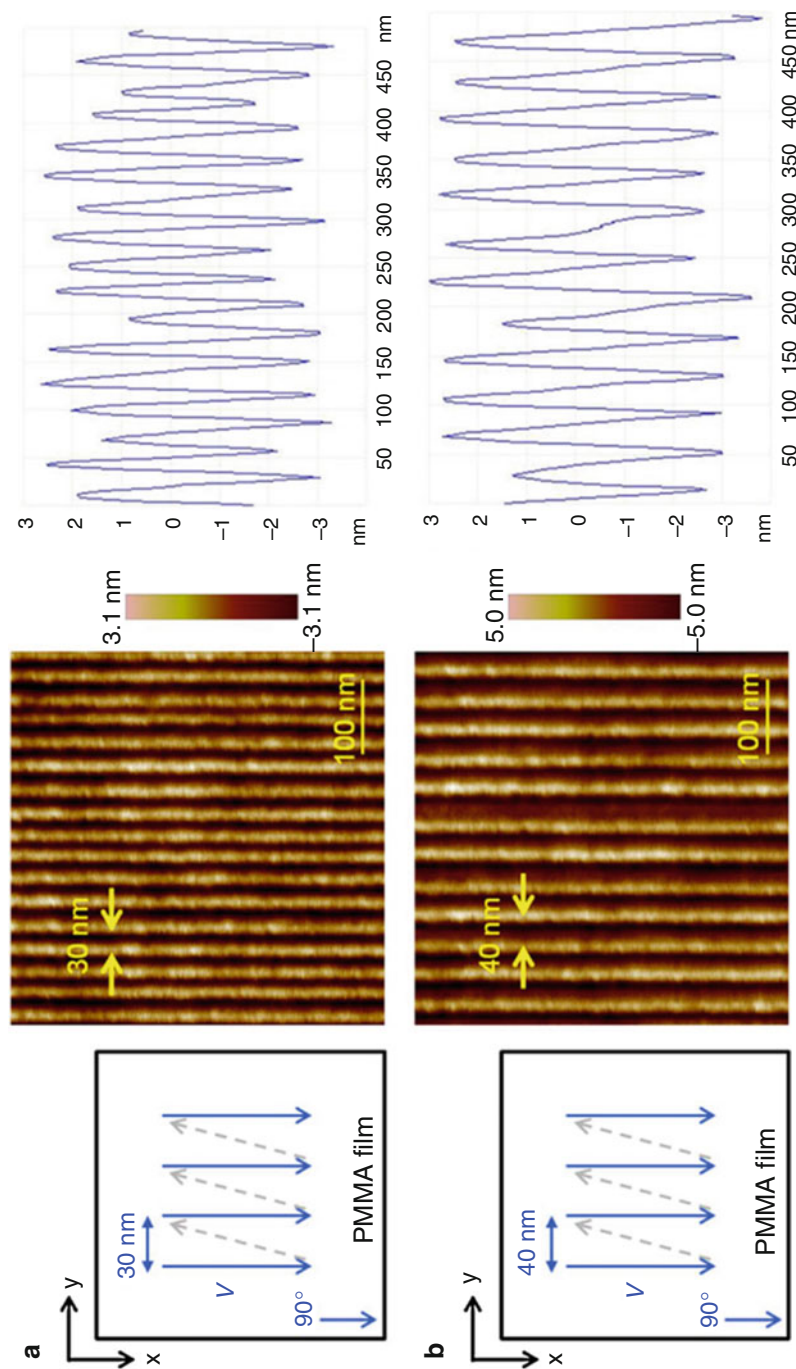
Fig. 19 Schematic of tip traces and AFM images of arrays of grooves obtained in the direction of 90° for a feed of (**a**) 30 nm and (**b**) 40 nm (Reproduced with permission from He et al. 2018)

influence on the formation of the ripple nanostructure. The relationship between the period and amplitude of the ripple nanostructure and the machining parameters can be obtained by the experimental tests.

4. The last method described in this chapter is just considered simply combining the material pileup and the machined groove to form a 3D nanostructure. The waveform of the structure is controlled by the separation distance between parallel adjacent scratching paths. Comparing these methods mentioned above, this approach shows the properties of high efficiency, easy operation, and high feasibility for various applications.

Although the AFM tip-based nanomechanical machining technique has already been used for the fabrication of 3D nanostructure, it is still in its infancy for the applications in many fields. Thus, much research in this area is needed to be considered.

1. *Fabrication 3D nanostructure on curved surface* To date, nanogroove and nanopit structures have been fabricated on the micro-ball, which has the potential to prepare the inertial confinement fusion (ICF) target with the expected dimension defects (Geng et al. 2017b). However, more complex nanostructures, such as 3D nanostructures, are required to simulate the arbitrary defects to advance the ICF field. Thus, in the future, 3D nanostructure on the curved surface can be machined by combination of the methods described in this chapter and the new device proposed in (Geng et al. 2017b).

2. *Promotion of the application* Using this technique, complex 3D nanostructure with expected dominations has already been fabricated successfully. However, no research related to the application of the 3D nanostructure machined by this technique has been reported yet. Thus, in the future, more attention should be given to the combination of this technique with other micro-/nanofabrication methods, such as wet etching, lift-off process, and optical lithography, to gain more interesting results, which can advance the application of this technique.

3. *Combination of multiple recourse effects* The mechanical effect combining the chemical and thermal energy or other recourses may lead to reducing the tip wear and improving the processing efficiency. This can contribute to create novel nanofabrication approaches.

References

Aoike T, Uehara H, Yamanobe T et al (2001) Comparison of macro- and nanotribological behavior with surface plastic deformation of polystyrene. Langmuir 17(7):2153–2159

Barton RA, Ilic B, Verbridge SS et al (2010) Fabrication of a nanomechanical mass sensor containing a nanofluidic channel. Nano Lett 10:2058–2063

Bhushan B (2002) Introduction to tribology. Wiley, New York

Binning G, Quate CF, Gerber C (1986) Atomic force microscope. Phys Rev Lett 56(9):930–933

Bowden FP, Tabor D (1950) The friction and lubrication of solids. Oxford University Press, Oxford

Brousseau EB, Arnal B, Thiery S, et al (2013) Towards CNC automation in AFM probe-based nano machining. In: International conference on micromanufacture, Victoria, p 95

Chen J, Workman RK, Sarid D et al (1994) Numerical simulations of a scanning force microscope with a large-amplitude vibrating cantilever. Nanotechnology 5(4):199–204

D'Acunto M, Napolitano S, Pingue P et al (2007) Fast formation of ripples induced by AFM: a new method for patterning polymers on nanoscale. Mater Lett 61:3305–3309

Dagata JA (1995) Device fabrication by scanned probe oxidation. Science 270(5242):1625–1626

Dinelli F, Leggett GJ, Shipway PH (2005) Nanowear of polystyrene surfaces: molecular entanglement and bundle formation. Nanotechnology 16(6):675–682

Dregely D, Neubrech F, Duan H et al (2013) Vibrational near-field mapping of planar and buried three-dimensional plasmonic nanostructures. Nat Commun 4:2237

Duan C, Alibakhshi MA, Kim DK et al (2016) Label-free electrical detection of enzymatic reactions in nanochannels. ACS Nano 10:7476–7484

Elkaakour Z, Aime JP, Bouhacina T et al (1994) Bundle formation of polymers with an atomic-force microscope in contact mode-a friction versus peeling process. Phys Rev Lett 73(24):3231

Geng Y, Yan Y, Zhao X et al (2013a) Fabrication of millimeter scale nanochannels using the AFM tip-based nanomachining method. Appl Surf Sci 266:386–394

Geng YQ, Yan YD, Xing YM et al (2013b) Modelling and experimental study of machined depth in AFM-based milling of nanochannels. Int J Mach Tools Manuf 73:87–96

Geng Y, Yan Y, Yu Y et al (2014) Depth prediction model of nanogrooves fabricated by AFM-based multi-pass scratching method. Appl Surf Sci 313:615–623

Geng Y, Yan Y, Hu Z et al (2016a) Investigation of the nanoscale elastic recovery of a polymer using an atomic force microscopy-based method. Meas Sci Technol 27:015001

Geng Y, Yan Y, Brousseau E et al (2016b) Processing outcomes of the AFM probe-based machining approach with different feed directions. Precis Eng 46:288–300

Geng Y, Yan Y, Brousseau E et al (2016c) Machining complex three-dimensional nanostructures with an atomic force microscope through the frequency control of the tip reciprocating motions. J Manuf Sci Eng 138:124501

Geng Y, Yan Y, Brousseau E et al (2017a) AFM tip-based mechanical nanomachining of 3D micro and nano-structures via the control of the scratching trajectory. J Mater Process Technol 248:236–248

Geng Y, Wang Y, Yan Y et al (2017b) A novel AFM-based 5-axis nanoscale machine tool for fabrication of nanostructures on a micro ball. Rev Sci Instrum 88(11):115109

He Y, Yan Y, Geng Y et al (2018) Fabrication of periodic nanostructures using dynamic plowing lithography with the tip of an atomic force microscope. Appl Surf Sci 427:1076–1083

Heyde M, Rademann K, Cappella B et al (2001) Dynamic plowing nanolithography on poly-methylmethacrylate using an atomic force microscope. Rev Sci Instrum 72:136–141

Kim SJ, Li LD, Han J (2009) Amplified electro kinetic response by concentration polarization near nanofluidic channel. Langmuir 25(13):7759–7765

Kumar K, Duan H, Hegde RS et al (2012) Printing colors at the optical diffraction limit. Nat Nanotechnol 7(9):557–561

Liang X, Chou SY (2008) Nanogap detector inside nanofluidic channel for fast real-time label-free DNA analysis. Nano Lett 8(5):1472–1476

Lin ZC, Hsu YC (2012) A calculating method for the fewest cutting passes on sapphire substrate at a certain depth using specific down force energy with an AFM probe. J Mater Process Technol 212:2321–2331

Liu W, Yan Y, Hu Z et al (2012) Study on the nano machining process with a vibrating AFM tip on the polymer surface. Appl Surf Sci 258:2620–2626

Mao Y, Kuo K, Tseng C et al (2009) Research on three dimensional machining effects using atomic force microscope. Rev Sci Instrum 80:0651056

Menard LD, Ramsey JM (2011) Fabrication of sub-5 nm nanochannels in insulating substrates using focused ion beam milling. Nano Lett 11(2):512–517

Peng R, Li D (2016) Fabrication of polydimethylsiloxane (PDMS) nanofluidic chips with controllable channel size and spacing. Lab Chip 16:3767–3776

Pires D, Hedrick JL, Silva AD et al (2010) Nanoscale three-dimensional patterning of molecular resists by scanning probes. Science 328:732–735

Richard DP, Jin Z, Feng X et al (1999) 'Dip-pen' nanolithography. Science 283(5402):661–663

Salapaka MV, Chen DJ, Cleveland JP (2000) Linearity of amplitude and phasein tapping-mode atomic force microscopy. Phys Rev B 61(2):1106–1115

Sun Y, Yan Y, Hu Z et al (2012) 3D polymer nanostructures fabrication by AFM tip-based single scanning with a harder cantilever. Tribol Int 47:44–49

Surtchev M, de Souza NR, Jerome B (2005) The initial stages of the wearing process of thin polystyrene films studied by atomic force microscopy. Nanotechnology 16(8):1213–1220

Tamayo J, Garcia R (1996) Deformation: contact time, and phase contrast in tapping mode scanning force microscopy. Langmuir 12(18):4430–4435

Yan Y, Hu Z, Zhao X et al (2010) Top-down nanomechanical machining of three-dimensional nanostructures by atomic force microscopy. Small 6(6):724–728

Yan Y, Sun Y, Yang Y et al (2012) Effects of the AFM tip trace on nanobundles formation on the polymer surface. Appl Surf Sci 258:9656–9663

Yan Y, Sun Y, Li J et al (2014) Controlled nanodot fabrication by rippling polycarbonate surface using an AFM diamond tip. Nanoscale Res Lett 9:372

Yan Y, Geng Y, Hu Z (2015) Recent advances in AFM tip-based nanomechanical machining. Int J Mach Tools Manuf 99:1–18

Yan Y, Cui X, Geng Y et al (2017) Effect of scratching trajectory and feeding direction on formation of ripple structure on polycarbonate sheet using AFM tip-based nanomachining process. Micro Nano Lett 12(12):1011–1015

Yang S, Yan Y, Liang Y et al (2013) Effect of the molecular weight on deformation states of the polystyrene film by AFM single scanning. Scanning 35(5):308–315

Zhan DP, Han LH, Zhang J et al (2016) Confined chemical etching for electrochemical machining with nanoscale accuracy. Acc Chem Res 49(11):2596–2604